Ultrasonics - Sonochemistry 70 (2021) 105292

Contents lists available at ScienceDirect

Ultrasonics - Sonochemistry

journal homepage: www.elsevier.com/locate/ultson

Ultrasound-assisted exfoliation of a layered 2D coordination polymer with HER electrocatalytic activity

Noemí Contreras-Pereda[a], Faezeh Moghzi[b], Javier Baselga[a], Haixia Zhong[c], Jan Janczak[d], Janet Soleimannejad[b], Renhao Dong[c], Daniel Ruiz-Molina[a,*]

[a] Catalan Institute of Nanoscience and Nanotechnology (ICN2), CSIC and BIST, Campus UAB, Bellaterra, 08193 Barcelona, Spain
[b] School of Chemistry, College of Science, University of Tehran, PO Box 14155-6455, Tehran, Iran
[c] Center for Advancing Electronics Dresden (Cfaed) and Faculty of Chemistry and Food Chemistry, Technische Universität Dresden, 01062 Dresden, Germany
[d] Institute of Low Temperature and Structure Research, Polish Academy of Science, Okólna 2, 50-950 Wroclaw, Poland

ARTICLE INFO

Keywords:
2D MOF
Coordination polymer
Nanomaterials
Delamination
Ultrasound
Catalysis

ABSTRACT

Large blue rectangular crystals of the 2D layered coordination polymer **1** have been obtained. The interest for this complex is two-fold. First, complex **1** is made of 2D layers packing along the (0–11) direction favored by the presence of lattice and coordinated water molecules. And second, nanostructures that could be derived by delamination are potentially suitable for catalytic purposes. Therefore it represents an excellent example to study the role of interlayer solvent molecules on the ultrasound-assisted delamination of functionally-active 2D metal-organic frameworks in water, a field of growing interest. With this aim, ultrasound-assisted delamination of the crystals was optimized with time, leading to stable nanosheet colloidal water suspensions with very homogeneous dimensions. Alternative bottom-up synthesis of related nanocrystals under ultrasound sonication yielded similar shaped crystals with much higher size dispersions. Finally, experimental results evidence that the nanostructures have higher catalytic activities in comparison to their bulk counterparts, due to larger metallic center exposition. These outcomes confirm that the combination of liquid phase exfoliation and a suitable synthetic design of 2D coordination polymers represents a very fruitful approach for the synthesis of functional nanosheets with an enhancement of catalytic active sites, and in general, with boosted functional properties.

1. Introduction

Metal-organic frameworks (MOFs), and overall coordination polymers, represent a class of crystalline materials embracing metal ions/clusters connected by organic ligands [1]. Profiting from their well-defined structures, high specific surface area and structural/chemical diversity, these materials have attracted great attention for gas storage/separation [2,3], catalysis [4], and sensor applications [5]. They can also exhibit abundant active sites and tuneable redox states, which lay the foundation for their applications in electrochemical energy storage/conversion, such as batteries [6], supercapacitors [7,8], water splitting [9] and oxygen reduction reactions [10]. However, though successful, most of these materials are generally synthesized as a bulk powder. Accordingly, a mass of active sites are buried and inaccessible for charge carriers, leading to sluggish ion diffusion and low utilization of active sites [11]. The apparent electrochemical performance has been therefore limited compared with predicted theoretical values. In contrast, thin nanosheets (NSs) possess a range of fascinating attributes including higher surface areas and sufficient accessible active sites, and their nanoscale thicknesses provide short ion/electron migration length owing to the quantum confinement effect [12]. Nonetheless, the synthetic methodology for NSs is in its fledgling stage, with many researchers actively endeavouring nowadays novel approaches to tune the structure/property interface. This is crucial before any application becomes a reality.

Between them, the development of thin NSs with enhanced electrochemical energy storage/conversion performance is an attractive opportunity. To date, a great effort has been dedicated to synthesize ultrathin NSs [13,14], including top-down physical [15] and chemical delamination [16,17], as well as bottom-up interface-assisted synthesis [18,19] and template-assisted synthesis [19]. Nevertheless, despite the success, these synthetic approaches still reveal limitations such as low yields or require of additional cleaning or annealing steps. Recently, we reported the synthesis of NSs, from 2D coordination polymers with interlayer solvent molecules, in high yields and control over their size and morphology using a Liquid Phase Exfoliation (LPE) process [20].

* Corresponding author.
E-mail address: dani.ruiz@icn2.cat (D. Ruiz-Molina).

https://doi.org/10.1016/j.ultsonch.2020.105292
Received 9 May 2020; Received in revised form 10 July 2020; Accepted 25 July 2020
Available online 30 July 2020

This result, together with other studies [16,17,21–24], has clearly demonstrated the importance of properly selecting the mixture of solvent and ultrasounds for a good delamination process. Overall, seemly candidates for LPE processes present weak interactions between layers due to occluded interlayer molecules that can be easily uninvolved under sonication in the appropriate solvent [25].

Herein we do demonstrate how such information can be put into practice to obtain stable colloidal dispersions of NSs in water with enhanced catalytic properties. As a proof-of-concept, we have selected the previously reported complex $[Cu(2,5pydc)(H_2O)]_n{\cdot}2H_2O$ (**1**), where 2,5pydc stands for 2,5-pyridine dicarboxylic acid [26]. The structure is made of Cu(II) ions coordinated to the carboxylic and pyridine groups of the 2,5pydc ligand forming 2D layers while water solvent molecules help to stabilize the 3D packing through hydrogen bonds. On top of that, complex **1** has a high density of metallic centres suitable for electrocatalytic activity. Initially, effort was put to obtain large crystals of complex **1** suitable for delamination using a complementary nickel salt as a template. Subsequent ultrasound-assisted exfoliation resulted in a suspension of rectangular shape and micrometre-long lateral sized nanosheets with a quite monodispersed size distribution. Such good distribution was impossible to obtain using bulk synthetic approaches under sonication. Finally, the catalytic activity in the hydrogen evolution reaction (HER) of the resulting NSs was tested [9,27]; enhancement on the density of exposed active sites after exfoliation boosts a higher HER electrocatalytic activity in base electrolyte compared to the bulk candidates. A schematic representation of both the exfoliation process and the catalytic activity of the resulting NSs is given in Fig. 1.

2. Results and discussion

2.1. Synthesis and characterization of large crystals of complex 1

First attempts to obtain crystals of complex **1** large enough to be delaminated were done following a methodology slightly different to that previously described [26]. In a typical experiment, an aqueous solution of 2,5pydc and triethylamine was mixed with an aqueous solution of $Cu(CH_3COO)_2{\cdot}4H_2O$ at room temperature for one day. Resulting blue crystals were washed with water and ethanol, dried under vacuum and chemically characterized as complex **1** by Fourier-Transformed Infrared spectroscopy (FT-IR) and powder X-Ray diffraction (PXRD) (see Fig. S1, Supporting information). The rectangular shaped crystals though have lateral dimensions inferior to 10–15 μm, too small to be subjected to the LPE process (Fig. 2). Serendipitously we found that addition of the $Ni(NO_3)_2{\cdot}6H_2O$ salt to the aqueous solution of 2,5pydc and triethylamine previous reaction with the Cu $(CH_3COO)_2{\cdot}4H_2O$ aqueous solution at room temperature for one day yielded much larger blue crystals susceptible to delamination, as shown in Fig. 2 (for experimental details see Materials section). Single crystal X-Ray diffraction (SXRD) confirmed the triclinic space group $P\bar{1}$ and the lattice parameters a = 4.7886 (6) Å, b = 7.6216 (5) Å, c = 13.7293 (8) Å, α = 99.390 (6)°, β = 98.762 (5)° and γ = 103.495 (7)°, characteristic of complex **1**. Moreover, the PXRD pattern of a bulk sample washed and dried is in perfect agreement with the simulated from the SXRD of complex **1** as well as the corresponding FT-IR spectrum (Fig. S2, Supporting information). Further, the presence of Cu as metallic center (with no or residual of nickel ions) was confirmed by Energy-dispersive X-ray spectroscopy (EDX) (Fig. S3a, Supporting information). And last but not least, thermal stability in ambient conditions was assessed with Thermogravimetric Analysis (TGA) (Fig. S3b, Supporting information). Complex **1** showcase a high thermal stability from room temperature to 100 °C. After exceeding 100–140 °C, a weight loss of 12.74% is observed corresponding to the evaporation of solvation water molecules in complex **1**. It is only beyond 260–270 °C that complex **1** thermally decomposes.

Interestingly, reaction of the $Ni(NO_3)_2{\cdot}6H_2O$ salt with an aqueous solution of 2,5pydc and triethylamine, exactly under the same experimental conditions previously described but in the absence of the copper salt (experimental details are given in the Experimental Section), yielded the new monomeric complex **2**. Complex **2** crystallizes in the $P2_1/c$ group where discrete molecular units establish a 3D supramolecular network through weak hydrogen bonds (Fig. 3). The crystallographic data and structure refinement details from SXRD are presented in Tables S1 and S2 (Supporting information). The lattice parameters of the structure are a = 5.3133(4) Å, b = 23.8147(14) Å, c = 7.2158(8) Å, α = 90°, β = 104.880(9)° and γ = 90°. The Ni metallic center is coordinated to two 2,5pydc in a bidentate mode, as

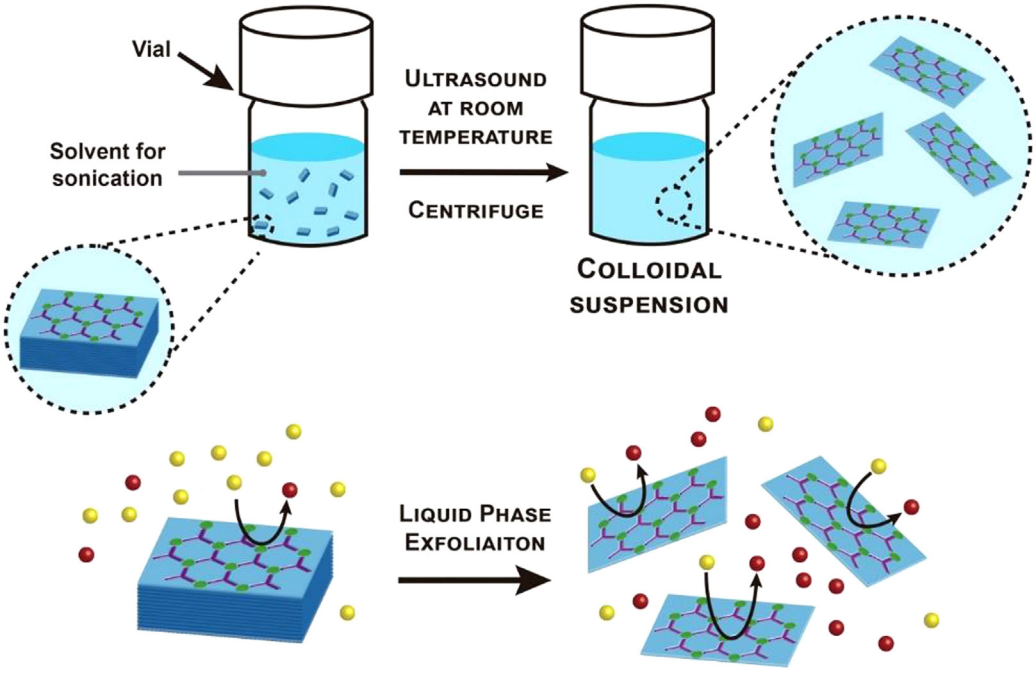

Fig. 1. (Top) Schematic representation of the ultrasound-assisted LPE process for the delamination of **1**, resulting in the formation of colloidal NS suspensions of **1**. (Bottom) Exfoliated NSs with LPE process present more catalytic active sites than bulk material.

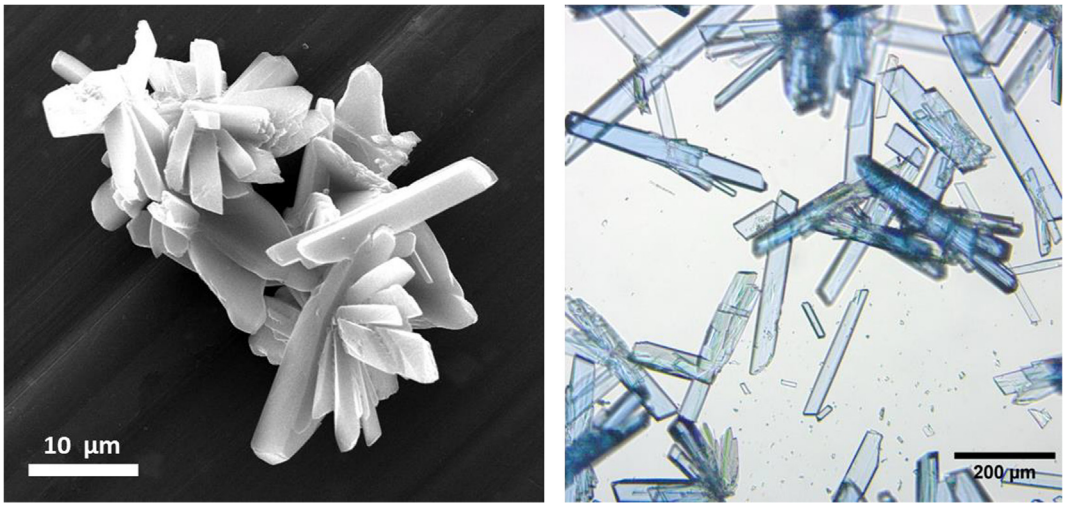

Fig. 2. (Left) SEM images of crystals of complex **1** synthetized as reported; (Right) Optical image of crystals of complex **1**, which can be stored over long periods of time, dried or dipped in water, without any loss of the crystalline phase.

the pyridyl and the 2-positioned carboxylic acid are involved in the coordination in equatorial positions. Two water molecules are coordinated to the Ni in the axial positions completing an octahedral coordination sphere. Hydrogen bonds between carboxylic groups and lattice water molecules ensure the good packing of **2** (Fig. 3b). Lattice and coordinated water molecules and 5-positionned carboxylic groups are involved in hydrogen bonding, packing the organo-metallic molecule into a three dimensional (3D) supramolecular network structure (for more information see Table S3, Supporting information). FT-IR spectroscopy confirmed the coordination in **2** (Fig. S4). As seen in the spectra, the characteristic bands of the COO^- at $\nu = 1597\ cm^{-1}$ and $\nu = 1386\ cm^{-1}$ are shifted to $v = 1602\ cm^{-1}$ and $v = 1397\ cm^{-1}$ respectively in the spectrum of **2**. Interestingly, the $1602\ cm^{-1}$ band is splitting into two peaks, one of them landing at $\nu = 1593\ cm^{-1}$ proving the coordination to the metal ligand is through only one of the carboxylic groups.

2.2. Structural analysis of complex *1*

Even though the crystal structure of complex **1** was already described, herein we revise in detail the supramolecular packing of the 2D layers due its relevance on the choice of solvent for the ultrasound-assisted delamination. The asymmetric unit of complex **1** consists of one crystallographically independent Cu(II) atom, one 2,5pydc ligand, one

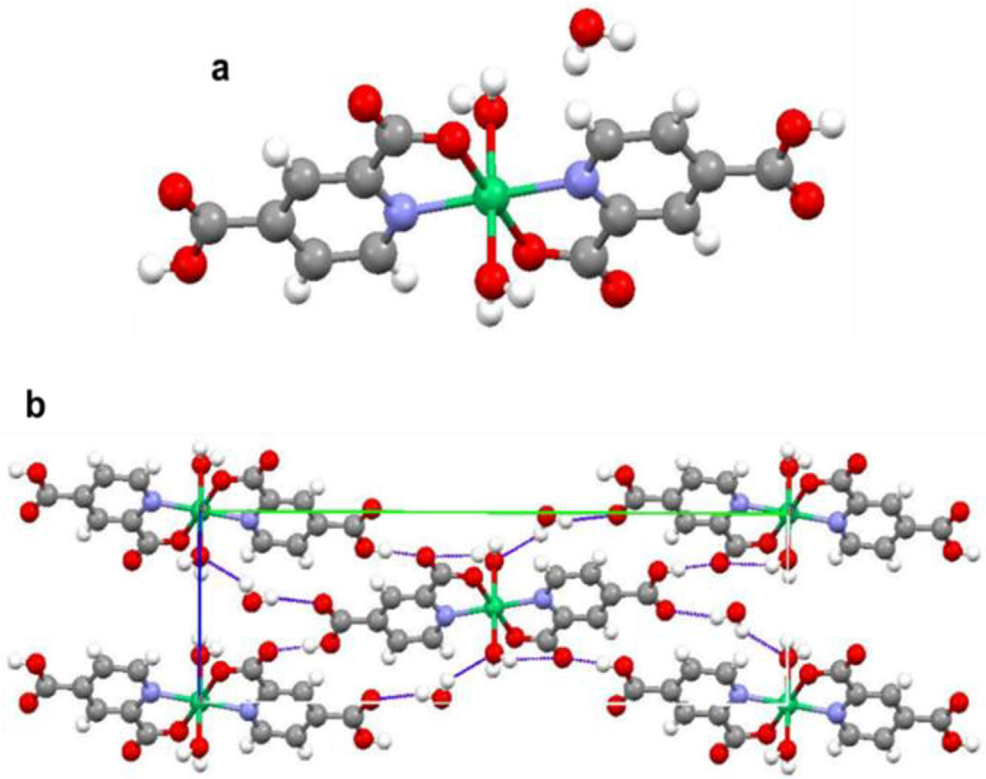

Fig. 3. (a) Unit cell of complex **2**; (b) Crystal packing of **2** mediated mainly by hydrogen bonds, displayed in green, between carboxylic groups and lattice water molecules.

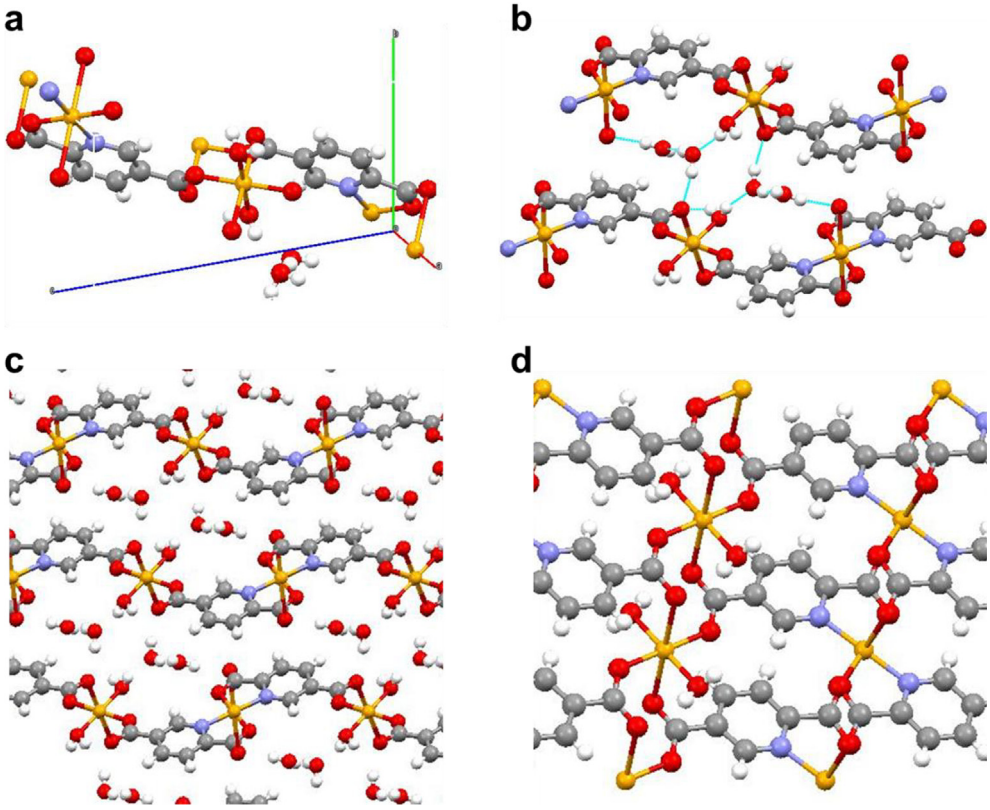

Fig. 4. (a) Image of the unit cell of **1** showing the crystallographic axis; (b) Side view of two layers of **1** showing lattice water molecules interconnecting them. Hydrogen bonds are displayed in blue showing the zig-zag configuration (c) Image of the crystallographic arrangement of the 2D layers in complex **1** obtained from a side view; (d) Top view of a 2D layer displaying the one dimensional chain arrangement of Cu ions.

water molecule coordinated to the metallic center and two lattice water molecule (see Fig. 4a). As we can observe in Fig. S5 (Supporting information), two different types of Cu(II) metallic centers can be found in the structure with octahedral coordination. The first metallic center Cu1 (Fig. S5a) is coordinated to four different 2,5pydc ligands through their 5-positionned carboxylic groups in equatorial positions. The axial positions of Cu1 are occupied by two water molecules. On the other hand, the second metallic center Cu2 (Fig. S5b), is coordinated to two 2,5pydc in a bidentate mode, as the pyridyl and the 2-positioned carboxylic acid are involved in the coordination, and to two 2,5pydc in a monodentate mode with 2 positioned carboxylic acid.

Thus, in complex **1**, the ligand 2,5pydc exhibits two kinds of bonding modes. One type of bonding involves O, N atoms and another is metallo-carboxylate monodentate bonding. As we can see in Fig. 4d, two O atoms from two monodentate coordination site form μ-oxo bridges that link the two adjacent Cu(II) ions. This leads to a rigid one-dimensional long straight chain of octahedral Cu(II) ions. Top view of a single layer can be found on Fig. 4d. Fig. 4c shows the packing of the 2D layers from a side view which extends the structure to the final crystalline lattice according to the SXRD measurements. The layers pack along the (0–11) direction with an interlayer distance of 7.002 Å. Lattice water molecule and coordinated water molecules are involved in hydrogen bonding, packing the layers into a three dimensional (3D) supramolecular network structure. Information on the different hydrogen bonds found in complex **1** is summarized in Table S4. The lattice water molecules allow the interconnection of the 2D layers displaying strong H-bonds (with short distances of 1.8–1.9 Å) in a zig-zag configuration (Fig. 4b).

2.3. Ultrasound-assisted delamination of complex *1*

Crystal delamination was attempted in five different solvents (acetone, DMF, ethanol, methanol and water) for 60 min while aliquots at 10, 20, 40 and 60 min were taken and analyzed by Scanning Electron Microscopy (SEM) to track the evolution with time (see Figs. S6 and S7, Supporting information). First attempts to delaminate complex **1** in acetone, DMF, ethanol and methanol were unsuccessful in spite of all the different experiments tested. In all the cases fragmentation in smaller crystals with less defined morphologies were found from where only a small fraction of flakes was identified (see Fig. S7, Supporting information). More successful were the different attempts to delaminate crystals of **1** in water. More in detail, after 10 min of sonication in water no NSs but initial symptoms of fragmentation are observed. After increasing the sonication time to 20 min, crystals start to lose their morphology while the population of micro-/nanostructures becomes more evident after 40 min of sonication, though large chunks of crystal still remain noticeable. It is only after 60 min of sonication that most of the macroscopic material disappears and the delamination yield increases (see Fig. S6 in Supporting information).

Finally, the few remaining non-exfoliated material was eliminated from the sample at 60 min after centrifuge. The resulting colloidal dispersion shows a characteristic Tyndall effect (Fig. 5a) and turned out to be stable at least for a week, as confirmed by DLS measurement (Fig. 5b). SEM images of an evaporated sample exhibit quite a monodispersed distribution of rectangular NSs of **1** with micrometer-long lateral distances and morphologies similar to those found for the bulk crystals (see Fig. 5c). Analysis of the images obtained by tilting the sample holder 70° showcase quite uniform thicknesses (Fig. 5d and Fig. S8) of 126 ± 35 nm (N = 45) indicating a high homogeneity on the NSs suspension.

FT-IR of drop-casted flakes (Fig. S9) corroborated the chemical stability of **1** during its nanostructuration through the exfoliation process as stretching vibrations corresponding to C-N and C-O are seen in the same positions of complex **1**. Further presence of Cu in the NSs was proved by EDX analysis (Fig. S9). Drop-casted flakes were analyzed as well by PXRD. As can be observed there, only two peaks appear in the diffraction pattern of the flakes, matching with two peaks of the diffraction pattern of **1**. Remarkably, the first of these two peaks correspond to the plane (0,1, − 1) which is the plane inner to the 2D layers in the crystallographic structure of **1** (see Fig. S9). It should be noticed

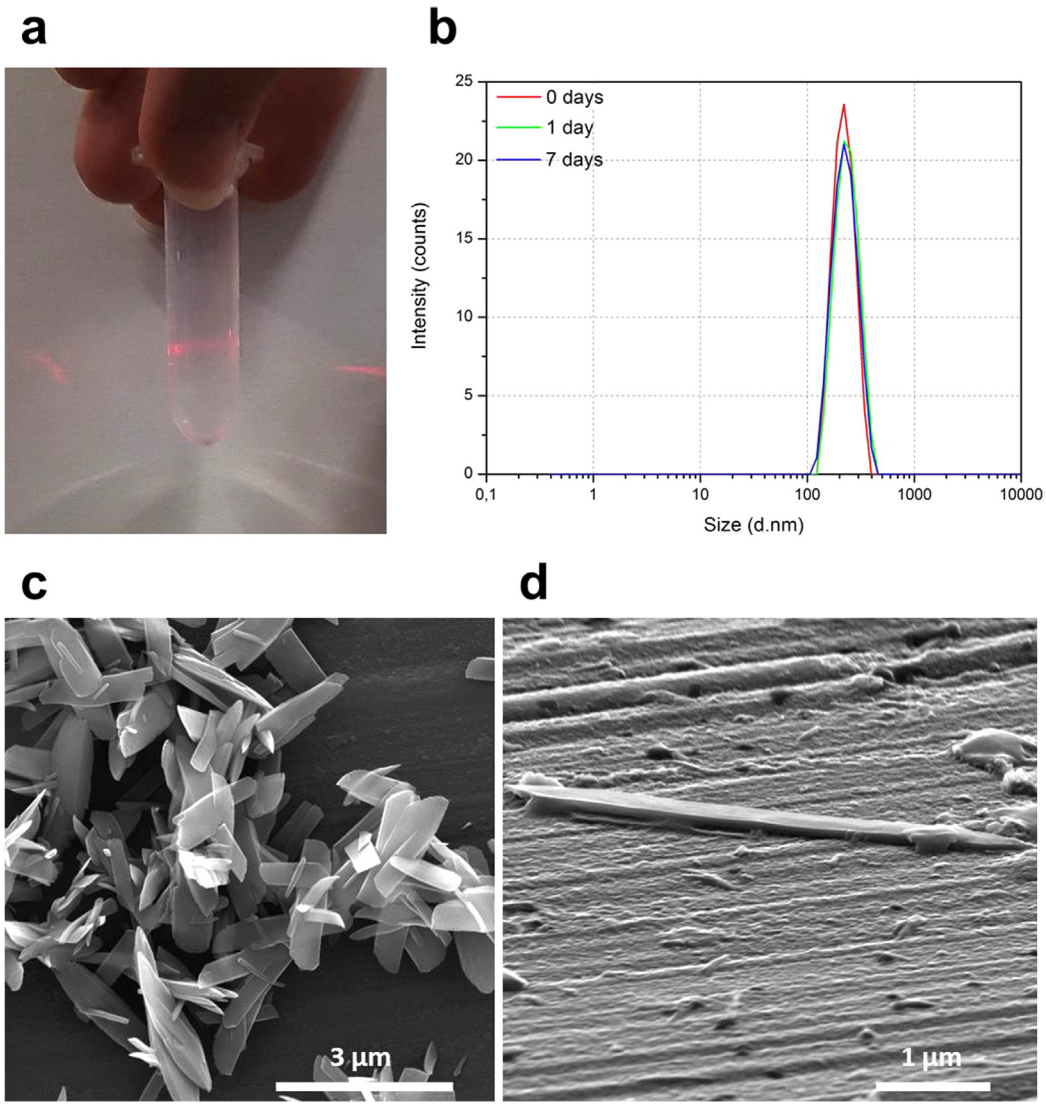

Fig. 5. As-centrifuged NSs after LPE process of complex **1** in water sonicating 60 min: (a) Image of an aqueous colloidal suspension after centrifuge showing Tyndall effect; (b) DLS measurement of a colloidal suspension of flakes taken as-exfoliated and centrifuged, after 1 day and after 7 days of exfoliations. The measurement remains basically unaltered over the whole period. (c) SEM image of the aqueous colloidal suspension showing only exfoliated NSs. Bulk materials were removed from the suspension by centrifuge (d) Tilted SEM image of NSs of **1** showing uniform thicknesses.

that intensity of all the other peaks from complex **1** is strongly suppressed in the pattern from the flakes because of the reduced size of these. Finally, elemental analysis results were in excellent agreement with those expected for the theoretical formula [Cu2,5pydc]·5.4 H_2O confirming that the NSs retain the composition of **1** (Theor. % C 25.78, % H 4.27; % N 4.29; Exptal. % C 25.84, % H 2.76, % N 3.89; Fit Error: 1.57%).

Just for comparison purposes, attempts to obtain similar rectangular flakes following a bottom-up synthesis were done using the same experimental conditions than those used for the bulk material but assisted with ultrasounds, a bottom-up approach already used for the synthesis of nanoscale coordination polymers (for additional details see Experimental Section) [28–30]. Remarkably, FT-IR spectra of the resulting crystals proved the coordination of the 2,5pydc with a metallic center as the same shifts previously seen in crystals of **1** are observed (Fig. 6c). Moreover, PXRD pattern of the nanocrystals matches with the simulated one from SXRD data (Fig. 6d). The resulting crystals present micrometer scale lateral sizes but thicker thicknesses and specially a much broad distribution with thicknesses ranging from 50 to 200 nm (Fig. 6a and b). This is corroborated by the presence of all peaks in the PXRD as nanostructuration of all crystals would lead to suppression of some of the peaks. Hence, bottom-up strategies involving sonication did not allow the direct and large yielded synthesis of NSs with a monodispersed distribution of sizes as the delamination process.

2.4. Electrochemical analysis

The electrocatalytic performance of as-prepared samples toward HER was estimated in a three-electrode cell in N_2-sataurated 1 M KOH electrolyte, wherein the carbon paper (CP) loading with catalyst is applied as the working electrode. As shown in Fig. 7a, the NS of **1** demonstrate a higher HER performance of more positive onset potential and dramatically larger current density (*j*) compared to the bulk counterpart sample, which is likely due to the increased density of exposed catalytic sites and improved electron transfer kinetics after the exfoliation. The overpotential (η) of the flake sample is 340 mV to deliver a current density of 10 mA cm^{-2}, far exceeding that of the bulk sample (530 mV), which is even comparable with the typical Ni/Co based MOF electrocatalyst for HER (Table 1). It is worth noting that the CP shows negligible HER current density even at large overpotential, revealing that CP acts as the current collector rather than contributing to the catalytic activity of the complex **1** NS electrode.

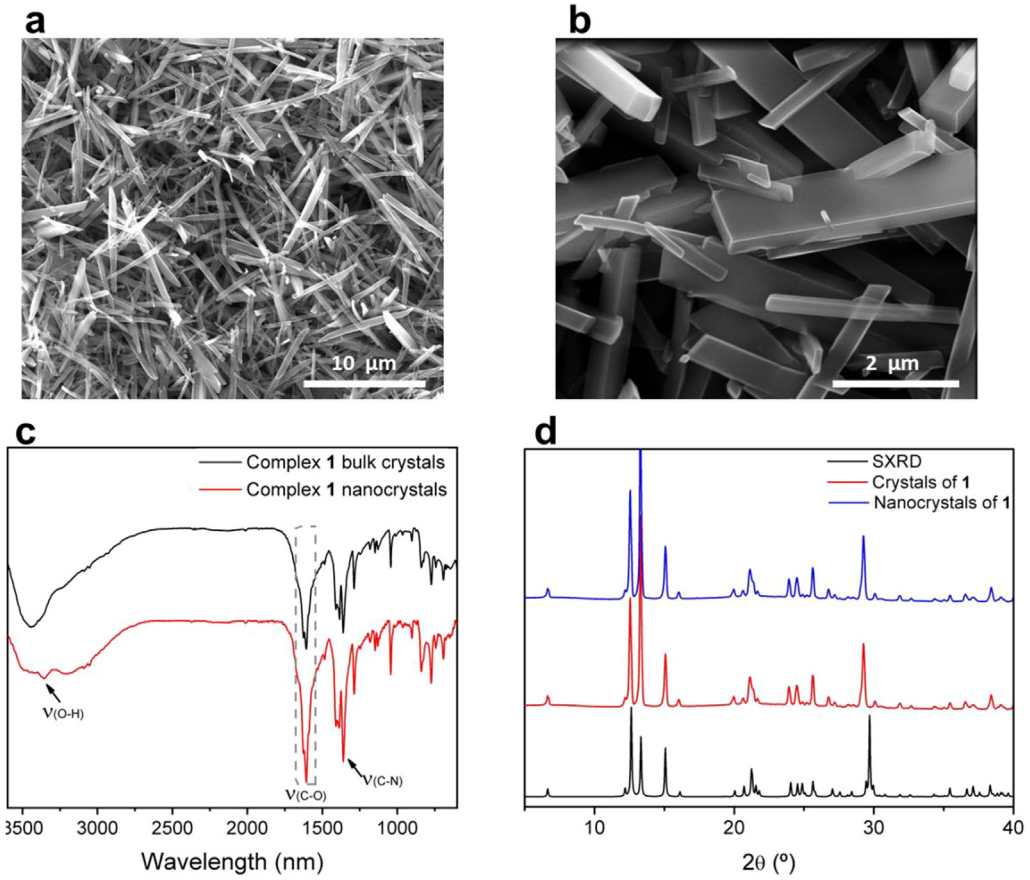

Fig. 6. (a) SEM image of nanocrystals of complex **1**; (b) Higher magnification SEM image of nanocrystals of **1** showing a wide distribution of sizes; (c) FT-IR spectra of 2,5pydc before the reaction (black) and of nanocrystals of **1** (red); (d) Comparison of the PXRD spectra of crystals of **1** and nanocrystals of **1** with the SXRD of **1**.

The Tafel slope (Fig. 7b) of the NSs catalyst was calculated to be as low as 70 mV dec^{-1}, which is lower than that of bulk counterpart (86 mV dec^{-1}), indicating the faster kinetics and the Volmer Heyrovsky mechanism at the NSs electrocatalyst during the HER process (Tafel slope is between 40 and 120 mV dec^{-1}). In term of Volmer-Heyrovsky mechanism, HER is proceeded through transferring one electron to the absorbed hydrogen and thus coupling of one proton at the surface of catalysts. Furthermore, electrochemical impedance spectroscopy (EIS) was performed to investigate the electron transfer kinetics. The results (Fig. 7c) verify the faster electron transfer kinetics of the HER process at the flakes electrode compared to the bulk catalyst and CP. As another important parameter for the practical application of HER electrocatalyst, the stability measurement was also carried out at complex **1** NS electrode. As displayed in Fig. 7d, only trace change ($\Delta\eta$ = 22 mV) of the overpotential at 10 mA cm^{-2} is observed for the NSs sample after 1000 potential cycles, highlighting its good stability for HER. Therefore, the exfoliation of the bulk materials into 2D NSs is indeed an effective strategy to create more exposed catalytic sites, expedite the electron transfer between the catalytic sites and electrode, and thus enhance the electrocatalytic activity.

3. Conclusions

A copper-based 2D coordination polymer has been synthesized and characterized. The structure of $[Cu(2,5pydc)(H_2O)]_n{\cdot}2H_2O$ (**1**) showed Cu(II) ions coordinated in two modes to the carboxylic and pyridine groups forming a linear high dense packing of metallic centers along the 2D layers. Occluded water solvent molecules stabilized the structure through hydrogen bonds interactions, turning **1** into a suitable candidate for LPE exfoliation.

Exfoliation of complex **1** was achieved in water applying local and large power ultrasounds for 60 min. The resulting suspension showcased NSs of **1** with rectangular shape and micrometer-long lateral sizes. LPE process provided quite monodispersed distribution of thicknesses, with values close to 100 nm. Chemical and structural characterization proved the high stability of the NSs during the delamination and ultrasound applying indicating the retention of high density of metallic center. Enhancement on the density of exposed active sites of **1** after exfoliation was confirmed using HER electrochemical analysis. A sufficient electron transfer between the catalytic sites and the current collector is thus allowed, which is accounting for the enhanced catalytic activity of 2D NSs compared to the bulk counterparts. Thus, our results evidence a higher catalytic activity using NSs of **1** when compared to bulk crystals of **1** as more positive overpotentials and larger currents are obtained. Further, faster electron kinetics are obtained using NS of **1** as expected for large exposed surface areas. Moreover, NSs of **1** show a high stability over many HER measurements.

4. Materials and methods

4.1. Chemicals and materials

Nickel nitrate hexahydrate salt, pyridine-2,5-dicarboxylic acid (2,5-pydc) and copper acetate monohydrate were purchased in Sigma Aldrich.

4.2. Synthesis of $\{[Cu(2,5\text{-}pydc)(H_2O)].2H_2O\}_n$ (1)

360 mg of 2,5-pydc were dissolved in 150 mL of water under reflux at 50 °C. After dissolving, 0.4 mmol of trimethylamine and a solution of

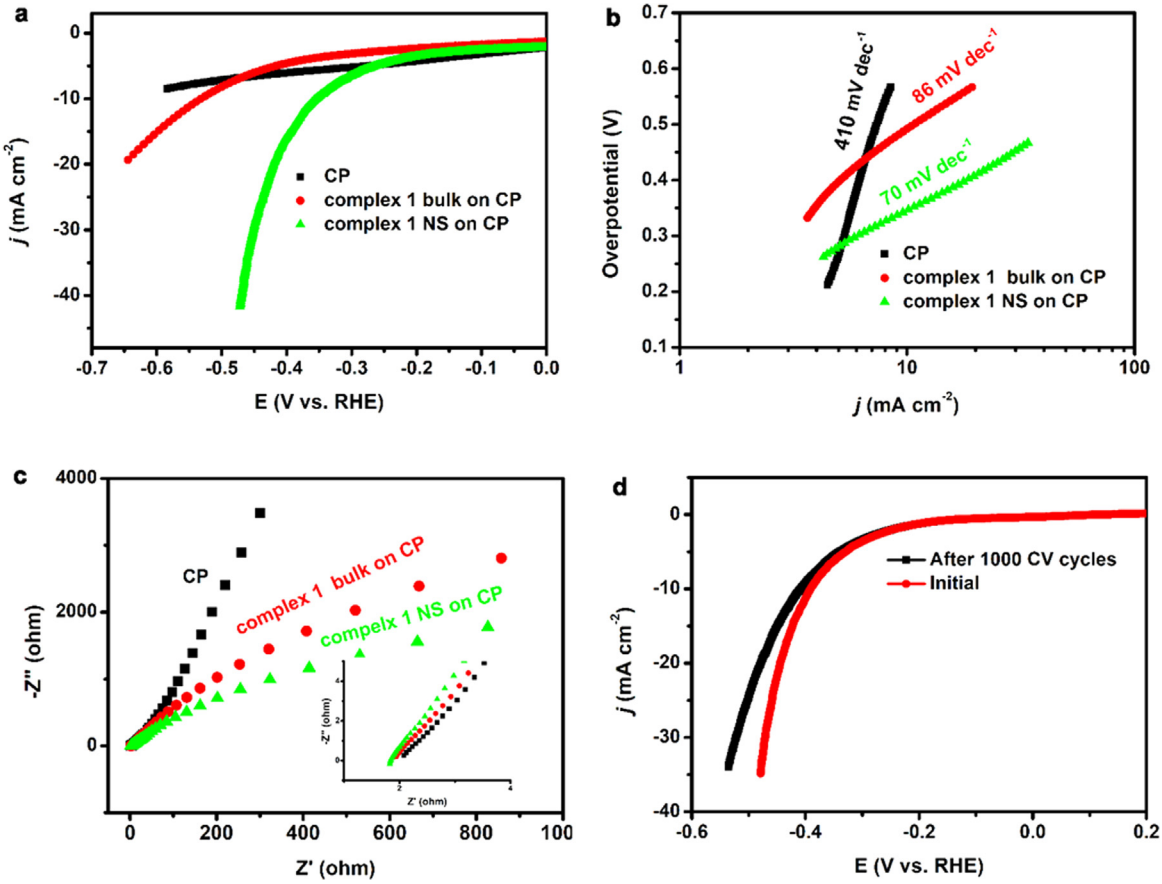

Fig. 7. Electrocatalytic performance of complex **1** bulk on CP (carbon paper), complex **1** NS on CP and CP in 1 M KOH. (a) HER polarization plots with IR compensation (i: current, R: resistant); (b) The corresponding Tafel plot; (c) EIS; (d) HER polarization curves of complex **1** NSs on CP before and after 1000 potential cycles. All HER polarization curves are IR-compensation.

Table 1
Comparison of HER catalytic activity of NS of **1** and other MOF based HER electrocatalysts.

Materials	Active centre	η mV (at 10 mA cm^{-2})	Tafel slope (mV dec^{-1})	Ref.
NS of **1**	Cu-N	340	70	This work
2D CTGU-5	Co(II)-O	388	125	[31]
AB &CTGU-5	Co(II)-O	44	45	
NiFe-MOF	Ni-O	134	34	[9]
THTA-Co	S-Co-N	283	71	[32]
THTNi 2DSP	Ni-S	333	80.5	[18]
CoBHT	Co-S	185	88	[33]
NiBHT	Ni-S	331	67	
MOS1	Co-S	340	149	[4]
NiAT	N-Ni-S	370	128	[34]
NENU-500	Mo-O	237	96	[35]

300 mg $Ni(NO_3)_2{\cdot}6H_2O$ in 50 mL of water were sequentially added. A solution of 200 mg of $Cu(CH_3COO)_2{\cdot}H_2O$ in 20 mL of water was added to above-mentioned mixture. The overall is kept close at room temperature. After one day, blue crystals for X-ray crystallography were obtained. Crystals were washed with water and ethanol and dried under vacuum. FT-IR (KBr pellet, cm^{-1}): 3357 (w), 3194 (w), 1626 (s), 1409 (m), 1386 (m), 1360 (s), 1288 (m), 1182 (w), 1148 (w), 1130 (w), 1044 (m), 902 (w), 840 (m), 773 (m), 743 (w), 692 (w). Elemental analysis calculated for $[C_7H_3CuO_4N]_n{\cdot}3.17H_2O$: C, 29.94%, H, 3.35%, N, 4.99%. Found: C, 29.81%, H, 2.84%, N, 4.93%.

4.3. Synthesis of complex $[C_{14}H_{12}NiO_{10}N_2]n{\cdot}2H_2O$ (2)

A solution of $Ni(NO_3){\cdot}6H_2O$ (30 mg, 0.1 mmol) in 5 mL water was added to a mixture of 2,5pydc acid (36 mg, 0.2 mmol) and triethylamine (0.4 mmol) in 15 mL water. The resulting solution was filtered and yellow crystals of complex **2** for X-ray crystallography were obtained by slow evaporation after 3 days. FT-IR (KBr pellet, cm^{-1}): 3316 (s), 1730 (m), 1642 (s), 1593 (m), 1486 (w), 1413 (w), 1384 (s), 1290 (w), 1120 (w), 1036 (w), 855 (m), 793 (m), 763 (m), 750 (m), 688 (w). Elemental analysis calculated for $[C_{14}H_{12}NiO_{10}N_2]n{\cdot}2H_2O$: C, 36.32%, H, 3.48%, N, 6.05%. Found: C, 35.58%, H, 4.01%, N, 6.25%. (Fit error: 0.93%). ICP %Ni: Theor. 12.68%; Expt. 12.43%.

4.4. Ultrasound-assisted synthesis of $\{[Cu(2,5\text{-}pydc)(H_2O)].2H_2O\}_n$ (1)

A mixture of 2,5pydc (0.4 mmol, 72 mg) and triethylamine (0.8 mmol) in 30 mL distilled water was stirred for 15 min to solve them. Then, 10 mL aqueous solution of $Ni(NO_3)_3{\cdot}6H_2O$ (0.2 mmol, 60 mg) was added. Then, a 40 mL aqueous solution of $Cu(CH_3COO)_2{\cdot}4H_2O$ (0.2 mmol, 40 mg) was added dropwise to the above-mentioned solution, while this last was being sonicated in ultrasound bath equipment (Elma S40H Elmasonic) with effective ultrasonic power of 140 W. After addition, the overall solution was sonicated for 15 min. After sonication, the obtained crystals were centrifuged for 2 min at 2000 rpm, washed with water and then dried under vacuum.

4.5. Liquid phase exfoliation

Delamination was performed with the LPE method assisted by

ultrasound. Exfoliation parameters like sonication time and used solvent were optimized. First, in order to optimize the sonication time and used solvent, 1 mg of crystals were dispersed in 4 mL of five solvents: DMF, ethanol, acetone, methanol and water. Ultrasounds were applied with a Branson Digital Sonifier SFX 550 (Emerson) sonicator equipped with a double step 1/8 in. microtip. This equipment has an effective ultrasonic power of 550 W. The microtip was immersed in the dispersions to produce the assistant ultrasound. The dispersions also were stirred to avoid sedimentation of the crystals and were kept at 20–25 °C by immersing it in a water-ice bath replacing it every 30 min. in order to avoid thermal decomposition. The temperature is measured periodically during the sonication. Ultrasounds were applied for 1 h in cycles of 2 min spaced by 30 s at 25% amplitude of the tip. Aliquots from every suspension were taken after 10 min, 20 min, 40 min and 60 min of sonication.

4.6. Isolation of 2D flakes

Non-exfoliated bulk crystals in suspension were removed by centrifugation. The flakes were remaining suspended in the supernatant. Aliquots from the suspensions were centrifuged for one minute at 7000 rpm. After delamination and centrifugation, the colloidal suspensions are kept under constant agitation in IKA HS 260 basic shaker. The complete exfoliation process was repeated with all the optimized parameters for full characterization of the obtained flakes.

4.7. Physico-chemical characterization of crystals

Optical images were obtained with a Zeiss Primo Star microscope equipped with a Zeiss Axiocam ERc 5 s camera on top. The software used for image acquirement was Zen Imaging Software (version ZEN 2012 blue edition). The crystals were dispersed on top of glassy and transparent microscope slides and put underneath the microscope. Powder X-ray diffraction (PXRD) patterns of the crystals were obtained with X'Pert3 Powder equipment (PANalytical), using Cu-Kα radiation. Intensity data were collected in continous-scan mode with a step size of 0,0334° and time per step of 160,02 s (speed 0,026526°/s). Data from the equipment was recorded and treated with X'Pert Data collector software (PANalytical). The obtained patterns were compared to the one from the resolved structure with single crystal X-ray diffraction (SXRD). SXRD of **1** and **2** was carried out using a Rigaku Oxford Diffraction: KUMA KM-4 diffractometer delivering a Mo microfocus radiation (λMo Kα 0.71073 Å) and equipped with a CrysAlis CCD detector. Fourier transform infrared spectroscopy (FT-IR) for both complexes was performed with Tensor 27 FT-IR spectrometer (Bruker) in attenuated total reflectance (ATR) mode. The instrument is equipped with a room temperature detector and a mid-IR source (4000 to 400 cm^{-1}). ATR was performed with a single window reflection of diamond model MKII Golden Gate, Specac. The spectra were recorded and treated with OPUS (Bruker) data collection software. Background spectrum in air was performed before the measurements, since the instrument is single beam. The dried samples were placed on the window reflection for measurement. Energy Dispersive X-ray Spectroscopy (EDX) technique was performed with SEM FEI Quanta 650F model (Thermo Fisher Scientific). The sample was prepared by drop-casting a diluted aqueous dispersion of crystals onto a metallic sample holder. Thermogravimetric analysis (TGA) was performed in a NETZSCH -STA 449 F1 Jupiter equipment in ambient atmosphere, applying a heating ramp of 25 to 350 °C at a constant rate of 10 °C/min. Inductively coupled plasma mass spectrometry (ICP-MS) ICP-MS was used for the determination of the nickel percentage in **2**. For the quantification of metal, a dilution 1:100 was necessary for detecting the correct signals. For ICP-MS analysis, atomic spectroscopic analytical standards were purchased from PerkinElmer Pure Plus. The isotope ^{58}Ni was selected as tracer. The nickel concentration of each sample was measured using a calibration curve obtained in the range of 0.01–250 ppm of metal. Standard reference material (PerkinElmer) with known values of nickel was analysed with each batch of samples. All the samples were measured per quadruplicate.

4.8. Physico-chemical characterization of flakes

Flakes were characterized by Scanning Electron Microscopy (SEM) with SEM FEI Quanta 650F microscope. The samples were prepared by drop-casting of the aliquots onto metallic sample holders. After evaporation of the solvent under ambient conditions, the previously suspended flakes remained on the holders. A 5 nm Pt layer was sputtered with Leica EM ACE600 on top of the samples, reproducing their topography. Afterwards, the particles were imaged with high acceleration voltages, between 10 and 20 kV at a working distance of 10 mm. Cross-section images were taken tilting the sample 70°. EDX was performed with SEM FEI Quanta 650F model. The sample was prepared by drop-casting of the aliquot suspension onto metallic sample holders. FT-IR of the flakes was performed with Hyperion 2000 FT-IR microscope (Bruker) working in reflexion mode. The instrument is equipped with a room temperature detector and a mid-IR source (4000 to 600 cm^{-1}). The spectra were recorded and treated with OPUS data collection software. Samples were prepared by drop-casting of the colloidal suspensions on top of gold substrates and left evaporated under ambient conditions. XRD measurements (theta-2theta scan) were performed in a Materials Research Diffractometer (MRD) from Malvern PANalytical company. This diffractometer has an horizontal omega-2theta goniometer (320 mm radius) in a four-circle geometry and it works with a ceramic X-ray tube with Cu Kα anode (λ = 1.540598 Å). The detector used is a Pixcel which is a fast X-ray detector based on Medipix2 technology. Stability of the flakes in colloidal suspension was studied by Dynamic Light Scattering (DLS) with Zetasizer Nano 3600 equipment (Malvern Instruments) at room temperature (20–25 °C). The data was collected with the Zetasizer 7.04 software. The samples were introduced in disposable plastic cuvettes and afterwards measured.

4.9. Electrochemical test

All the electrochemical tests were conducted in a three-electrode cell in 1 M KOH electrolyte, wherein carbon paper loading with catalysts, Ag/AgCl electrode and carbon rod were serviced as working electrode, reference electrode and counter electrode, respectively. Catalysts (1 mg) were dispersed into 200 μL of ethanol and 20 μL of Nafion solution by sonication for 30 min. Then, the catalyst inks were drop-casted on carbon paper giving a catalyst loading of ca. 1 mg cm^{-2}. Cyclic voltammetry (CV) tests were conducted in N_2-saturated 1 M KOH solution from −0.6 V to −1.6 V vs. Ag/AgCl with a scan rate of 10 mV s^{-1}. The accelerated durability tests were carried out with potential cycles from −0.6 to −1.6 V vs RHE with a sweep rate of 50 mV s^{-1}. The reference electrode was calibrated with respect to the reversible hydrogen electrode (RHE: $E_{RHE} = E_{Ag/AgCl} + 0.0592*pH + 0.197$). All HER polarization curves were corrected with IR-compensation. And the impedance was tested by electrochemical impedance spectroscopy (EIS) measurements with an AC voltage with 10 mV amplitude in a frequency range from 100 kHz to 0.1 Hz at open-circuit voltage.

Declaration of Competing Interest

The authors declare that they have no known competing financial interests or personal relationships that could have appeared to influence the work reported in this paper.

Acknowledgements

This work was supported by grant RTI2018-098027-B-C21 from the

Spanish Government funds and by the European Regional Development Fund (ERDF). The ICN2 is funded by the CERCA programme/ Generalitat de Catalunya. The ICN2 is supported by the Severo Ochoa Centres of Excellence programme, funded by the Spanish Research Agency (AEI, grant no. SEV-2017-0706). Noemí Contreras Pereda's project that gave rise to these results received the support of a fellowship from "laCaixa" Foundation (ID 100010434). The fellowship code is LCF/BQ/ES17/11600012. Renhao Dong acknowledgements the financial support from ERC Starting Grant (FC2DMOF, No. 852909) and DFG project (SPP 1928, COORNETs).

Appendix A. Supplementary data

Supplementary data to this article can be found online at https://doi.org/10.1016/j.ultsonch.2020.105292.

References

[1] H.C. Zhou, J.R. Long, O.M. Yaghi, Introduction to metal-organic frameworks, Chem. Rev. 112 (2012) 673–674, https://doi.org/10.1021/cr300014x.
[2] Y. Zhang, X. Feng, S. Yuan, J. Zhou, B. Wang, Challenges and recent advances in MOF-polymer composite membranes for gas separation, Inorg. Chem. Front. 3 (2016) 896–909, https://doi.org/10.1039/C6QI00042H.
[3] Y. Peng, Y. Li, Y. Ban, H. Jin, W. Jiao, X. Liu, W. Yang, Metal-organic framework nanosheets as building blocks for molecular sieving membranes, Science 346 (2014) 1356–1359, https://doi.org/10.1126/science.1254227.
[4] A.J. Clough, J.W. Yoo, M.H. Mecklenburg, S.C. Marinescu, Two-dimensional metal – organic surfaces for efficient hydrogen evolution from water, J. Am. Chem. Soc. 137 (2015) 118–121, https://doi.org/10.1021/ja5116937.
[5] M.G. Campbell, M. Dincă, Metal-organic frameworks as active materials in electronic sensor devices, Sensors 17 (2017) 1108, https://doi.org/10.3390/s17051108.
[6] D. Sheberla, J.C. Bachman, J.S. Elias, C.J. Sun, Y. Shao-Horn, M. Dincă, Conductive MOF electrodes for stable supercapacitors with high areal capacitance, Nat. Mater. 16 (2017) 220–224, https://doi.org/10.1038/nmat4766.
[7] W.-H. Li, K. Ding, H.-R. Tian, M.-S. Yao, B. Nath, W.-H. Deng, Y. Wang, G. Xu, Conductive metal-organic framework nanowire array electrodes for high-performance solid-state supercapacitors, Adv. Funct. Mater. 27 (2017) 1702067, https://doi.org/10.1021/ja5116937.
[8] D. Feng, T. Lei, M.R. Lukatskaya, J. Park, Z. Huang, M. Lee, L. Shaw, S. Chen, A.A. Yakovenko, A. Kulkarni, J. Xiao, K. Fredrickson, J.B. Tok, X. Zou, Y. Cui, Z. Bao, Robust and conductive two-dimensional metal-organic frameworks with exceptionally high volumetric and areal capacitance, Nat. Energy 3 (2018) 30–36, https://doi.org/10.1038/s41560-017-0044-5.
[9] J. Duan, S. Chen, C. Zhao, Ultrathin metal-organic framework array for efficient electrocatalytic water splitting, Nat. Commun. 8 (2017) 15341, https://doi.org/10.1038/ncomms15341.
[10] E.M. Miner, T. Fukushima, D. Sheberla, L. Sun, Y. Surendranath, M. Dincă, Electrochemical oxygen reduction catalysed by Ni3(hexaiminotriphenylene)2, Nat. Commun. 7 (2016) 10942, https://doi.org/10.1038/ncomms10942.
[11] H. Jin, C. Guo, X. Liu, J. Liu, A. Vasileff, Y. Jiao, Y. Zheng, S.-Z. Qiao, Emerging Two-Dimensional Nanomaterials for Electrocatalysis, Chem. Rev. 118 (2018) 6337–6408, https://doi.org/10.1021/acs.chemrev.7b00689.
[12] W. Zhao, J. Peng, W. Wang, S. Liu, Q. Zhao, W. Huang, Ultrathin two-dimensional metal-organic framework nanosheets for functional electronic devices, Coordin. Chem. Rev. 377 (2018) 44–63, https://doi.org/10.1016/j.ccr.2018.08.023.
[13] R. Sakamoto, K. Takada, X. Sun, T. Pal, T. Tsukamoto, E.J.H. Phua, A. Rapakousiou, K. Hoshiko, H. Nishihara, The coordination nanosheet (CONASH), Coordin. Chem. Rev. 320–321 (2016) 118–128, https://doi.org/10.1016/j.ccr.2015.12.001.
[14] L. Cao, T. Wang, C. Wang, Synthetic strategies for constructing two-dimensional metal-organic layers (MOLs): a tutorial review, Chin. J. Chem. 36 (2018) 754–764, https://doi.org/10.1002/cjoc.201800144.
[15] L.J. Han, D. Zheng, S.G. Chen, H.G. Zheng, J. Ma, A highly solvent-stable metal-organic framework nanosheet: morphology control, exfoliation, and luminescent property, Small 14 (2018) 1703873, https://doi.org/10.1002/smll.201703873.
[16] C. Kutzscher, A. Gelbert, S. Ehrling, C. Schenk, I. Senkovska, S. Kaskel, Amine assisted top-down delamination of the two-dimensional metal-organic framework Cu2(bdc)2, Dalton Trans. 46 (2017) 16480–16484, https://doi.org/10.1039/C7DT03890A.
[17] Y. Ding, Y.P. Chen, X. Zhang, L. Chen, Z. Dong, H.L. Jiang, H. Xu, H.C. Zhou, Controlled intercalation and chemical exfoliation of layered metal-organic frameworks using a chemically labile intercalating agent, J. Am. Chem. Soc. 139 (2017) 9136–9139, https://doi.org/10.1021/jacs.7b04829.
[18] R. Dong, M. Pfeffermann, H. Liang, Z. Zheng, X. Zhu, J. Zhang, X. Feng, Large-area, free-standing, two-dimensional supramolecular polymer single-layer sheets for highly efficient electrocatalytic hydrogen evolution, Angew. Chem. Int. Edit. 54 (2015) 12058–12063, https://doi.org/10.1002/anie.201506048.
[19] R. Dong, T. Zhang, X. Feng, Interface-assisted synthesis of 2D materials: trend and challenges, Chem. Rev. 118 (2018) 6189–6235, https://doi.org/10.1021/acs.chemrev.8b00056.
[20] N. Contreras-Pereda, P. Hayati, S. Suárez-García, L. Esrafili, P. Retailleau, S. Benmansour, F. Novio, A. Morsali, D. Ruiz-Molina, Delamination of 2D coordination polymers: the role of solvent and ultrasound, Ultrason.-Sonochem. 55 (2019) 186–195, https://doi.org/10.1016/j.ultsonch.2019.02.014.
[21] A. Gallego, C. Hermosa, O. Castillo, I. Berlanga, C.J. Gómez-García, E. Mateo-Martí, J.I. Martínez, F. Flores, C. Gómez-Navarro, J. Gómez-Herrero, S. Delgado, F. Zamora, Solvent-induced delamination of a multifunctional two dimensional coordination polymer, Adv. Mater. 25 (2013) 2141–2146, https://doi.org/10.1002/adma.201204676.
[22] S. Benmansour, A. Abhervé, P. Gómez-Claramunt, C. Vallés-García, C.J. Gómez-García, Nanosheets of two-dimensional magnetic and conducting Fe(II)/Fe(III) mixed-valence metal-organic frameworks, ACS Appl. Mater. Interfaces 9 (2017) 26210–26218, https://doi.org/10.1021/acsami.7b08322.
[23] S. Goswami, L. Ma, A.B.F. Martinson, M.R. Wasielewski, O.K. Farha, J.T. Hupp, Toward metal-organic framework-based solar cells: enhancing directional exciton transport by collapsing three-dimensional film structures, ACS Appl. Mater. Interfaces 8 (2016) 30863–30870, https://doi.org/10.1021/acsami.6b08552.
[24] B. Garai, A. Mallick, A. Das, R. Mukherjee, R. Banerjee, Self-exfoliated metal-organic nanosheets through hydrolytic unfolding of metal-organic polyhedra, Chem.-Eur. J. 23 (2017) 7361–7366, https://doi.org/10.1002/chem.201700848.
[25] S. Suárez-García, N.N. Adarsh, G. Molnár, A. Bousseksou, Y. Garcia, M.M. Dîrtu, J. Saiz-Poseu, R. Robles, P. Ordejón, D. Ruiz-Molina, Spin-crossover in an exfoliated 2D coordination polymer and its implementation in thermochromic films, ACS Appl. Nano Mater. 1 (6) (2018) 2662–2668, https://doi.org/10.1021/acsanm.8b00341.
[26] B. Rajasekhar, N. Bodavarapu, M. Sridevi, G. Thamizhselvi, K. RizhaNazar, R. Padmanaban, Toka Swu, Nonlinear optical and G-Quadruplex DNA stabilization properties of novel mixed ligand copper(II) complexes and coordination polymers: synthesis, structural characterization and computational studies, J. Mol. Struct. 1156 (2018) 690e699, https://doi.org/10.1016/j.molstruc.2017.11.103.
[27] J. Joyner, E.F. Oliveira, H. Yamaguchi, K. Kato, S. Vinod, D.S. Galvao, D. Salpekar, S. Roy, U. Martinez, Ch.S. Tiwary, S. Ozden, P.M. Ajayan, Graphene supported MoS2 structures with high defect density for an efficient HER electrocatalysts, ACS Appl. Mater. Interfaces 12 (11) (2020) 12629–12638, https://doi.org/10.1021/acsami.9b17713.
[28] P. Hayati, S. Suárez-García, A. Gutierrez, E. Şahin, D. Ruiz Molina, A. Morsali, A.R. Rezvani, Sonochemical synthesis of two novel Pb(II) 2D metal coordination polymer complexes: new precursor for facile fabrication of lead (II) oxide/bromide micro-nanostructures, Ultrason. Sonochem. 42 (2018) 310–319, https://doi.org/10.1016/j.ultsonch.2017.11.037.
[29] P. Hayati, S. Suárez-García, A. Gutiérrez, D. Ruiz Molina, A. Morsali, A.R. Rezvani, Sonochemical synthesis of a novel nanoscale 1D lead (II)$[Pb_2(L)_2(I)_4]$ n coordination Polymer, survey of temperature, reaction time parameters, Ultrason. Sonochem. 42 (2018) 320–326, https://doi.org/10.1016/j.ultsonch.2017.11.033.
[30] P. Hayati, A.R. Rezvani, A. Morsali, D. Ruiz-Molina, S. Geravand, S. Suárez-García, M.A. Moreno-Villaécija, S. García-Granda, R. Mendoza-Meroño, P. Retailleau, Sonochemical synthesis, characterization, and effects of temperature, power ultrasound and reaction time on the morphological properties of two new nanostructured mercury(II) coordination supramolecule compounds, Ultrason, Sonochem 37 (2017) 382–393, https://doi.org/10.1016/j.ultsonch.2017.01.021.
[31] Y.P. Wu, W. Zhou, J. Zhao, W.W. Dong, Y.Q. Lan, D.S. Li, C. Sun, X. Bu, Surfactant-assisted phase-selective synthesis of new cobalt MOFs and Their efficient electrocatalytic hydrogen evolution reaction, Angew. Chem. Int. Ed. Engl. 56 (42) (2017) 13001–13005, https://doi.org/10.1002/anie.201707238.
[32] R. Dong, Z. Zheng, D.C. Tranca, J. Zhang, N. Chandrasekhar, S. Liu, X. Zhuang, G. Seifert, X. Feng, Immobilizing molecular metal dithiolene-diamine complexes on2D metal-organic frameworks for electrocatalytic H_2 production, Chem. Eur. J. 23 (2017) 2255–2260, https://doi.org/10.1002/chem.201605337.
[33] C.A. Downes, A.J. Clough, K. Chen, J.W. Yoo, S.C. Marinescu, Evaluation of the H_2 evolving activity of benzenehexathiolate coordination frameworks and the effect of film thickness on H_2 production, ACS Appl. Mater. Interfaces 10 (2) (2018) 1719–1727, https://doi.org/10.1021/acsami.7b15969.
[34] X. Sun, K.-H. Wu, R. Sakamoto, T. Kusamoto, H. Maeda, X. Ni, W. Jiang, F. Liu, S. Sasaki, H. Masunaga, H. Nishihara, Bis(aminothiolato)nickel nanosheet as a redox switch for conductivity and an electrocatalyst for the hydrogen evolution reaction, Chem. Sci. 8 (2017) 8078–8085, https://doi.org/10.1039/c7sc02688a.
[35] J.-S. Qin, D.-Y. Du, W. Guan, X.-J. Bo, Y.-F. Li, L.-P. Guo, Z.-M. Su, Y.-Y. Wang, Y.-Q. Lan, H.-C. Zhou, Ultrastable polymolybdate-based metal-organic frameworks as highly active electrocatalysts for hydrogen generation from water, J. Am. Chem. Soc. 137 (22) (2015) 7169–7177, https://doi.org/10.1021/jacs.5b02688.